ELECTROCHEMISTRY

Direct electrosynthesis of pure aqueous H_2O_2 solutions up to 20% by weight using a solid electrolyte

Chuan Xia*, Yang Xia*, Peng Zhu, Lei Fan, Haotian Wang†

Hydrogen peroxide (H_2O_2) synthesis generally requires substantial postreaction purification. Here, we report a direct electrosynthesis strategy that delivers separate hydrogen (H_2) and oxygen (O_2) streams to an anode and cathode separated by a porous solid electrolyte, wherein the electrochemically generated H^+ and HO_2^- recombine to form pure aqueous H_2O_2 solutions. By optimizing a functionalized carbon black catalyst for two-electron oxygen reduction, we achieved >90% selectivity for pure H_2O_2 at current densities up to 200 milliamperes per square centimeter, which represents an H_2O_2 productivity of 3.4 millimoles per square centimeter per hour (3660 moles per kilogram of catalyst per hour). A wide range of concentrations of pure H_2O_2 solutions up to 20 weight % could be obtained by tuning the water flow rate through the solid electrolyte, and the catalyst retained activity and selectivity for 100 hours.

Hydrogen peroxide (H_2O_2) is a nexus chemical for a variety of industries, currently produced through the indirect, energy-demanding, and waste-intensive anthraquinone process (*1*, *2*). This traditional method usually generates H_2O_2 mixtures with concentrations of 1 to 2 weight % (wt %), necessitating further costly purifications and distillations to reach concentrations appropriate for commercial use (*3*). The overall process requires centralized infrastructure and thus relies heavily on transportation and storage of bulk H_2O_2 solutions, which are unstable and hazardous (*4*). Direct synthesis of H_2O_2 from a hydrogen (H_2) and oxygen (O_2) mixture (Fig. 1A) provides an alternative route for small-scale on-site generation (*5*–*7*). Catalyst development for this reaction has progressed over the past decade (*8*–*12*), exemplified by a palladium-tin catalyst with high selectivity (>95%) and productivity [61 moles per kilogram of catalyst (kg_{cat}) per hour] for H_2O_2 synthesis (*9*). However, a drawback of this route is the inherent flammability hazard associated with mixing high-pressure H_2 and O_2 (*13*). In practice, the H_2 feedstock must be heavily diluted using CO_2 or N_2 carrier gas, substantially lowering the yields of H_2O_2. In addition, the use of methanol solvent leads to extra purification costs in the preparation of pure aqueous H_2O_2 solutions.

By contrast, electrosynthesis of H_2O_2 can decouple the H_2/O_2 redox exchange into two half-cell reactions (Eqs. 1 and 2), followed by the ionic recombination process (Eq. 3):

$2e^-$ O_2 reduction reaction ($2e^-$-ORR):

$$O_2 + H_2O + 2e^- \rightarrow HO_2^- + OH^- \quad (1)$$

H_2 oxidation reaction (HOR):

$$H_2 \rightarrow 2H^+ + 2e^- \quad (2)$$

H_2O_2 formation:

$$HO_2^- + H^+ \rightarrow H_2O_2 \quad (3)$$

In the electrochemical process, O_2 and H_2 can be kept safely separated and introduced in pure form to accelerate the reaction. The synthesis can proceed under ambient conditions for on-site H_2O_2 generation and could potentially even output electricity. Although there have been selective catalysts such as noble metals or carbon materials developed for the $2e^-$ ORR pathway (*14*–*18*), the H_2O_2 product has typically been generated in a mixture, with solutes in traditional liquid electrolytes ranging from acidic to alkaline pH. Extra separation processes to recover pure H_2O_2 solutions were therefore required. Other designs including the use of deionized (DI) water or a polymer electrolyte membrane as the ion-conducting electrolyte have been explored on a preliminary basis for obtaining pure H_2O_2 solutions, but they generally suffered from low reaction rates, product concentrations, or Faradaic efficiencies (FEs) (supplementary text, note 1) (*19*–*21*).

Here, we report a porous solid electrolyte design to realize direct electrosynthesis of pure H_2O_2 solutions. As illustrated in Fig. 1B and figs. S1 and S2, independent H_2 and O_2 streams were respectively delivered to HOR and $2e^-$-ORR catalysts coating gas diffusion layer (GDL) electrodes. The anode and cathode "sandwiched" the cation exchange membrane (CEM) and anion exchange membrane (AEM) layers (see materials and methods for details) to avoid flooding by direct contact with liquid water. In the center, a thin and porous solid electrolyte layer facilitated ionic recombination of H^+ and HO_2^- ions crossing from the anode and cathode with small ohmic losses; a flowing DI water stream confined to this middle layer could then dissolve the pure H_2O_2 product with no introduction of ionic impurities. By tuning the HO_2^- generation rate or the DI water flow rate, a wide range of H_2O_2 concentrations (from hundreds of parts per million to tens of percent) could be directly obtained with no need for further energy-consuming downstream purification.

To deliver efficient conversion, electrocatalysts with high activity and selectivity for $2e^-$-ORR and HOR are a prerequisite. We chose the state-of-the-art platinum on carbon (Pt/C) catalyst for HOR at the anode, which affords high H_2-to-H^+ conversion rates at small overpotentials (*22*–*24*). For the cathode, however, electrocatalysts with high activity and selectivity for $2e^-$-ORR toward H_2O_2 have been much less thoroughly explored than the extensively studied fuel-cell catalysts for $4e^-$-ORR to H_2O. Recent studies on noble metal catalysts such as Au-Pd or Pd-Hg (*14*, *25*), as well as carbon materials such as graphene, carbon nanotubes, or porous carbon (*15*, *16*, *26*–*29*), have demonstrated high selectivity toward the $2e^-$ pathway. Nevertheless, practical current densities (hundreds of milliamperes per square centimeter) with high FEs, particularly at neutral pH for the purpose of pure H_2O_2 generation, have not yet been achieved. We chose commercial carbon black as the starting material because of its low cost, its high surface area (fig. S3) for high mass activity, and, especially, its nanoparticulate morphology (fig. S3) to facilitate O_2 diffusion from the GDL (layer-by-layer stacking of graphene nanosheets, by contrast, can hinder gas transport). Surface functional groups such as ethers (C–O–C) and carboxylic acids (HO–C=O) have previously been posited to activate the adjacent carbon atomic sites for selective $2e^-$-ORR (*15*, *16*). Hence, we treated the carbon black nanoparticles with nitric acid to introduce such oxidized functionality (see materials and methods and supplementary text, note 2). No morphological changes were observed for these carbon black nanoparticles after acid treatment (fig. S3); however, high-resolution x-ray photoelectron spectroscopy (XPS) (fig. S4) confirmed that acid treatment enriched the particles with oxygen-containing functional groups, including C–O–C/C–OH and HO–C=O, as deconvolved from carbon and oxygen 1*s* signals.

We found that surface oxidation strongly correlated with H_2O_2 selectivity and activity (fig. S5). The selectivity rose from <80% for the unoxidized particles to ~95% for even relatively low surface oxygen coverage (2.11%). Although the H_2O_2 selectivity was similar upon further increasing the surface oxygen coverage from 2.11 to 11.62% as shown in fig. S5B, we found that the $2e^-$-ORR catalytic activity gradually improved (fig. S5C), which we ascribe to the increased concentration of active sites. After optimization, we selected carbon black with ~10% surface oxygen coverage (CB-10%) as the

Department of Chemical and Biomolecular Engineering, Rice University, Houston, TX 77005, USA.
*These authors contributed equally to this work.
†Corresponding author. Email: htwang@rice.edu

cathode catalyst for further development of the full cell. We first used a standard three-electrode rotation ring-disc electrode (RRDE) system in neutral pH (0.1 M Na_2SO_4) to evaluate the intrinsic activity of CB-10% for benchmark comparisons (see materials and methods). The catalyst presented an impressive H_2O_2 generation performance, with a maximal H_2O_2 selectivity of ~98% and an onset potential of 0.438 V versus reversible hydrogen electrode (RHE), to deliver a 0.1 mA cm^{-2} H_2O_2 generation current (fig. S6, A and B). A flow-cell system with GDL electrodes and traditional liquid electrolytes was further used to test the catalyst's performance without O_2 gas diffusion limits in both neutral and alkaline electrolytes (fig. S6C). With a wide potential window to deliver high H_2O_2 selectivity (>90%) in both neutral and alkaline solutions, the catalyst reached maximal FE of 98 and 99%, respectively (fig. S6D), in good agreement with RRDE tests. Furthermore, H_2O_2 partial currents of ~300 mA cm^{-2} were achieved, whereas high FEs were still maintained in neutral solutions, better than the highest O_2-to-H_2O_2 conversion rates yet observed (*30*).

The porous solid electrolyte layer comprises either an anion or cation solid conductor, which can consist of ion-conducting polymers with different functional groups (*31*), inorganic compounds (*32*), or other types of solid electrolyte materials such as ceramics, polymer–ceramic hybrids, or solidified gels (*33*). Among these different solid conductors, polymer ion conductors have been widely used for electrochemistry applications because of their fast ion conduction at room temperature, high reliability, and ease of processing (*34*). Because proton conduction is generally faster than anion conduction (*35*), here, we chose to use styrene-divinylbenzene copolymer microspheres (fig. S7), functionalized with sulfonic acid groups for cation (H^+) conduction (*36*), as a representative solid electrolyte layer for demonstration. Those copolymer microspheres, once packed together in the middle layer, allow for H^+ conduction along their interconnected surfaces; in addition, the micrometer pores formed between these stacked spheres allow for DI water flow and product release (fig. S7). We first studied the impact of the solid electrolyte on H_2O_2 selectivity by the CB-10% catalyst in a standard three-electrode setup (fig. S8A), with potentials calibrated to the RHE scale. The results (fig. S8B) indicate that there were no obvious negative or positive impacts on H_2O_2 selectivity of the CB-10% catalyst when switching from traditional liquid electrolyte to our solid electrolyte. Next, we systematically investigated the H_2O_2 production performance of CB-10% using a two-electrode cell with porous solid electrolyte, as shown schematically in Fig. 1B. Figure 2A shows the current-voltage (*I-V*) curve of a CB-10%//SE//Pt-C cell with O_2 and H_2 gas streams delivered to the cathode and anode, respectively. The DI water flow rate was fixed at 27 ml $hour^{-1}$ for this 4-cm^2 electrode cell to prevent substantial product accumulation, particularly under large currents. H_2O_2 was readily detected starting from a cell voltage of −0.54 V, suggesting an early onset considering the equilibrium voltage of −0.76 V (*37*). The H_2O_2 selectivity remained >90% across the entire cell voltage range, reaching a maximum of 95% (Fig. 2B). An H_2O_2-generation current of ~30 mA cm^{-2}

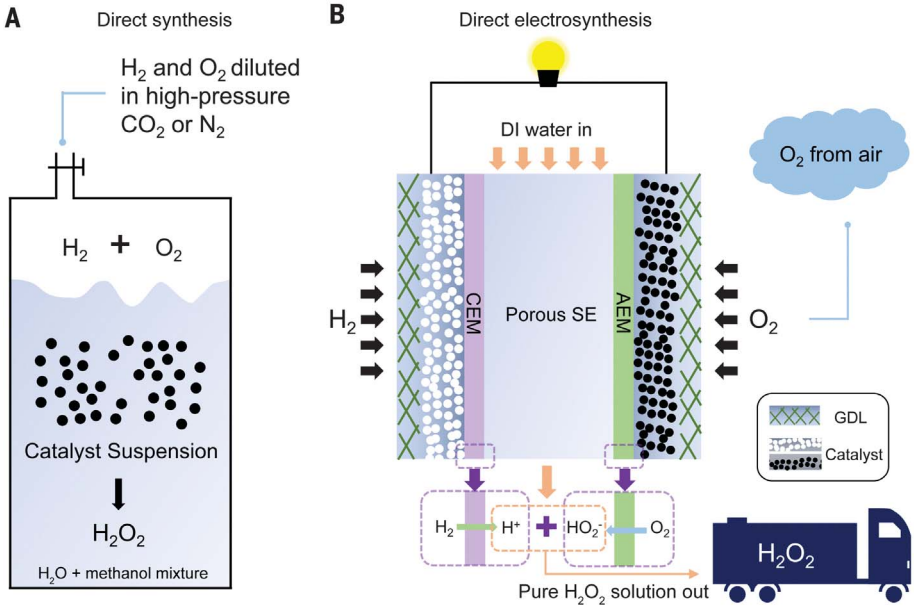

Fig. 1. Schematic illustration of the two different H_2O_2 synthesis methods using H_2 and O_2. (**A**) Synthesis of H_2O_2 using diluted H_2 and O_2 under high pressure. Methanol used to improve the solubility of the reacting gases in the medium (*44*) must then be removed downstream. Other studies that avoid alcohols have been performed in acidic solutions of either HCl or H_2SO_4, with NaBr or NaCl as promotors (*44*). (**B**) Electrosynthesis of H_2O_2 using pure H_2 and O_2 streams separately introduced to the anode and cathode, respectively. SE represents a solid electrolyte, which consisted in this study of either functionalized styrene–divinylbenzene copolymer microspheres or inorganic $Cs_xH_{3-x}PW_{12}O_{40}$ (see materials and methods). Electrochemically generated cations (H^+) and anions (HO_2^-), driven by the electric field, cross in the porous SE layer and recombine to form H_2O_2. DI water flowing through the porous SE layer then dissolves the H_2O_2 with no impurities.

Table 1. Performance metrics of different H_2O_2 generation methods

	Purity	Productivity (mol kg_{cat}^{-1} $hour^{-1}$)	Productivity (mmol cm^{-2} $hour^{-1}$)	Selectivity (%)	Stability	Max. concentration (ppm)
Our method	Pure	3660	3.4	90 ~ 95	>100 hours	200,000
Direct synthesis	Mixture (*8*, *9*, *45*–*47*)	60.8 ~ 180	N/A	80.7 ~ 96	Up to 4 cycles or 4 hours	5300
Electrochemical synthesis	Mixture (*48*–*53*)	N/A	0.05 ~ 1.2	47 ~ 93.5	2 ~ 6 hours	3400 ~ 60,000
	Pure (*19*–*21*)	N/A	0.16 ~ 0.289	26.5 ~ 30	6 ~ 72 hours	1400 ~ 80,000

(0.53 mmol cm^{-2} $hour^{-1}$) could be obtained under 0 V (no external energy input). Moreover, a potential of only 0.61 V was required to deliver a current density of 200 mA cm^{-2} with an H_2O_2 FE of ~90%. This current represents an H_2O_2-generation rate of 3.4 mmol cm^{-2} $hour^{-1}$, or 3660 mol kg_{cat}^{-1} $hour^{-1}$ considering both cathode and anode catalyst (see materials and methods; a comparison with literature benchmarks is given in Table 1 and fig. S9). No H_2 byproduct (potentially from H_2 evolution at large overpotentials) was detected from the cathode side under such a high current density (fig. S10A), indicating exclusive selectivity for ORR. Other types of solid electrolyte with different material properties, including polymeric conductors for HO_2^- conduction and inorganic $Cs_xH_{3-x}PW_{12}O_{40}$ for cation conduction, were also demonstrated to be effective for pure H_2O_2 solution generation (fig. S11), which suggests the wide tunability and versatility of our solid electrolyte design.

Under a fixed DI water flow rate of 27 ml $hour^{-1}$, the H_2O_2 concentration from our 4-cm^2

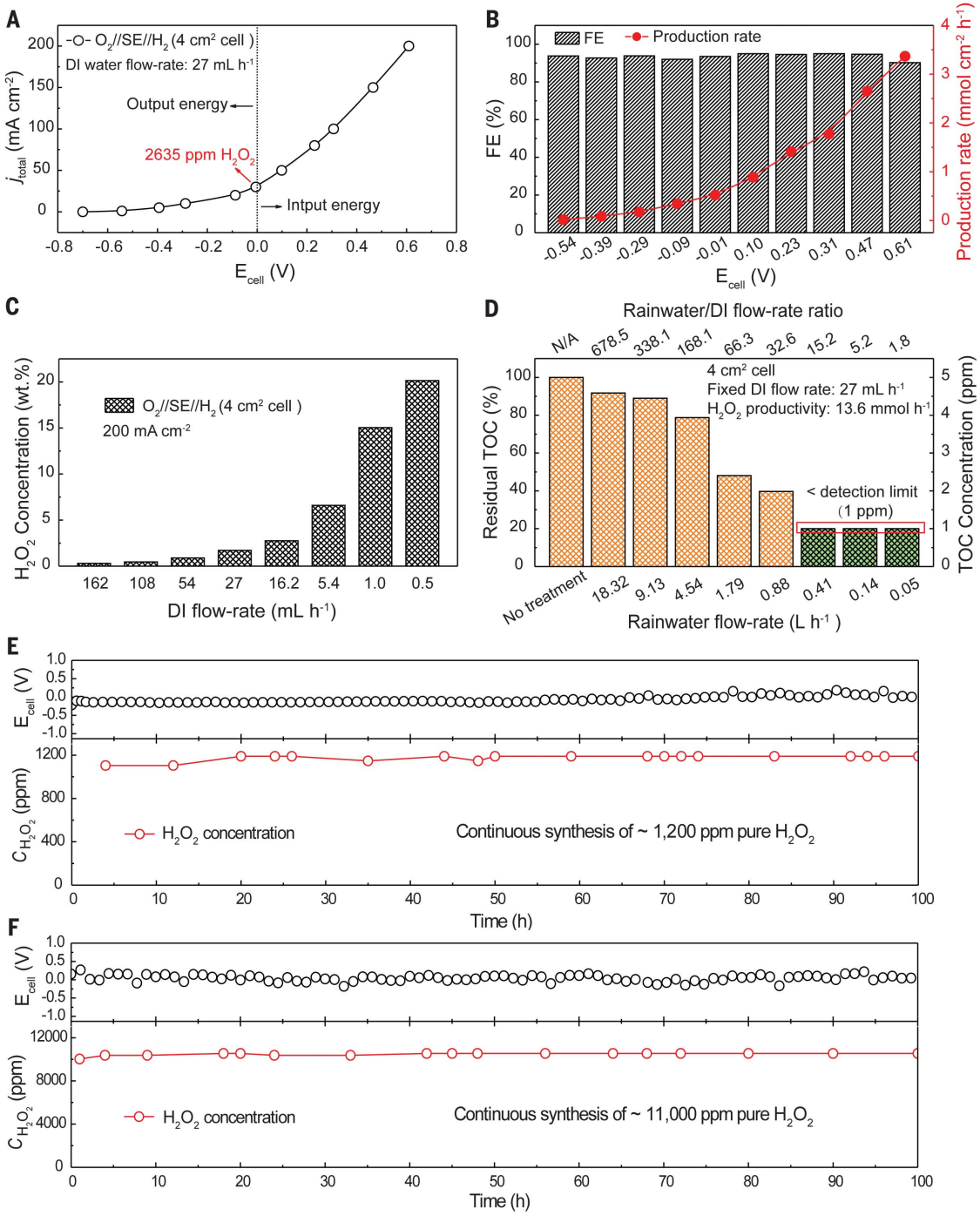

Fig. 2. Direct electrosynthesis of pure H_2O_2 using H_2 and O_2 with porous solid electrolyte. (**A**) *I-V* curve of CB-10%//SE//Pt-C cell with an H^+-conducting porous solid electrolyte. We define the cell voltage as negative when the cell can output energy during the production of H_2O_2. The positive cell voltage therefore indicates that energy input is required for the reactor. The cell voltages were *iR* (current × resistance) compensated (see materials and methods). (**B**) Corresponding FEs and production rates of H_2O_2 under different cell voltages. (**C**) Dependence of H_2O_2 concentration on the DI water flow rate at an overall current density of 200 mA cm^{-2}. Up to 20 wt % pure H_2O_2 solutions could be continuously generated for immediate use. The data points in (A) to (C) each represent the mean of two independent measurements. (**D**) Removal of TOC in Houston rainwater using the H_2O_2 solution generated at a fixed current density of 200 mA cm^{-2} and a fixed DI water flow rate of 27 ml $hour^{-1}$ in our 4-cm^2 electrode device. A high rainwater treatment rate of 0.88 liters $hour^{-1}$ (0.22 liters $cm^{-2}_{electrode}$ $hour^{-1}$ or 2200 liters $m^2_{electrode}$ $hour^{-1}$) was achieved to meet the drinking water standards (TOC < 2 ppm according to the Texas Commission on Environmental Quality). (**E** and **F**) Stability tests for continuous generation of pure H_2O_2 solutions with concentrations >1000 and 10,000 ppm, respectively. No degradation of cell voltage or H_2O_2 concentration was observed over the 100-hour continuous operation. The cell currents and DI flow rates were (E) 60 mA and 27 ml $hour^{-1}$ and (F) 120 mA and 5.4 ml $hour^{-1}$, respectively.

electrode cell reached ~1.7 wt % with an overall cell current of 800 mA. By speeding up or slowing down the DI water flow rate while maintaining the H_2O_2 generation current, we could tune product concentration over a wide range for different application scenarios (Fig. 2C). Up to 20 wt % [200,000 ppm] aqueous H_2O_2 solutions could be directly and continuously obtained by means of electrochemical synthesis. We noticed that the measured H_2O_2 selectivity decreased with increased H_2O_2 concentration (fig. S12A). We ascribe the observed decrease in apparent FE (98% at 0.3 wt % versus 70% at 6.6 wt %) to the following two possible processes. First, the higher concentration of H_2O_2 product in the solid electrolyte layer could shift the equilibrium of the $2e^-$-ORR while enhancing the selectivity of the competing $4e^-$ pathway to H_2O product, thereby lowering intrinsic H_2O_2 selectivity. Second, while H_2O_2 formation proceeds, a fraction of the generated H_2O_2 might not be detected, particularly at high product concentration, because of a potentially increased bimolecular decomposition rate and/or increased crossover to the anode, as frequently observed in methanol or formic acid fuel cells (*38*–*40*); this would result in an apparent decrease in H_2O_2 selectivity. Possible impurities in the product solution, such as sodium (common in water), iron (from the device), sulfur (from the SE), and platinum (from the anode), were quantified to be at or below ppm levels determined by inductively coupled plasma atomic emission spectroscopy (ICP-OES) (table S1 and supplementary text, note 3). Therefore, the electrochemically synthesized H_2O_2 solutions could be put to immediate use out of the cell without any further purification, lowering cost substantially compared with other methods and simplifying the setup for the deployment of on-site generation technology. Long-term stability is another important metric for evaluating catalysis. Our device produced ~1200 and ~11,000 ppm H_2O_2 solutions continuously in 100-hour test runs with no degradation in activity or selectivity (Fig. 2, E and F). XPS characterization of the CB-10% catalyst after the reaction revealed that the surface oxygen functionality was robust and did not appear to have been electrochemically reduced during the operation of the ORR (fig. S10B).

As a representative demonstration of on-site application, we used the as-synthesized H_2O_2 from our device for rainwater purification (Fig. 2D and fig. S13). Compared with traditionally used chlorine compounds, which may produce carcinogens in the processed drinking water (*41*), H_2O_2 is safe for both human and environmental health when disinfecting and decomposing organic contaminants, typically assessed as removal of total organic carbon (TOC) (*42*). The use of electrochemically generated H_2O_2 is not only economical (see supplementary text, note 4), but also avoids the transportation and storage of hazardous bulk H_2O_2. We directly mixed the generated H_2O_2 stream (200 mA cm^{-2}, 27 ml $hour^{-1}$ DI water flow) from our 4-cm^2 electrode device with the rainwater stream (feeding rate ranging from 18.32 to 0.05 liters $hour^{-1}$) to optimize the purification efficiency. The TOC of the pristine rainwater collected at the Rice University campus in Houston was detected to be ~5 ppm (see materials and methods), which is above the Texas treated-water standard of ~2 ppm (*43*). Decreasing the rainwater feeding rate gradually lowered the TOC remaining (Fig.

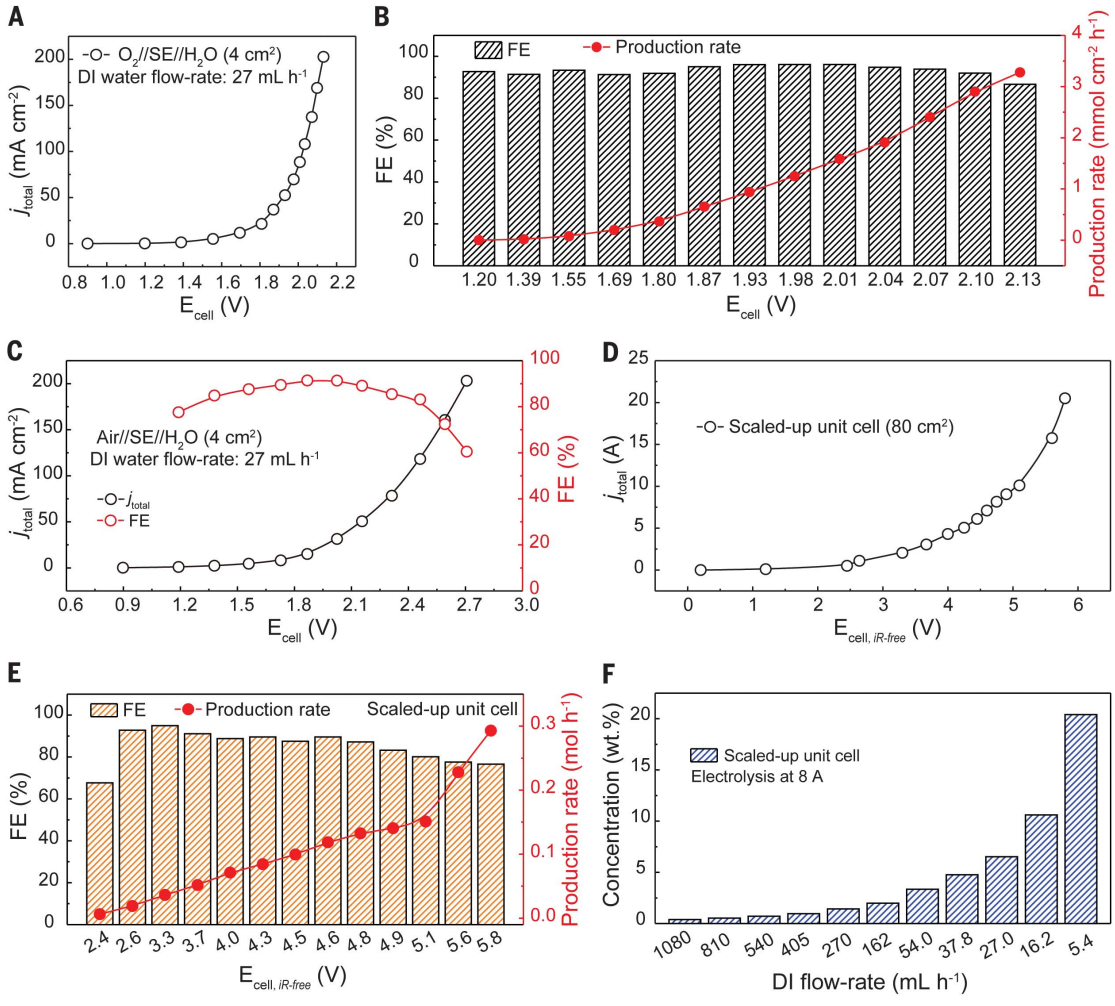

Fig. 3. Electrosynthesis of pure H_2O_2 solutions by $2e^-$-ORR and water oxidation. (**A**) *I-V* curve for an O_2//SE//H_2O cell in which H_2O is oxidized at the anode side to form protons and O_2. A 0.5 M aqueous H_2SO_4 solution was used to improve ionic conductivity on the anode side and was not consumed during electrosynthesis. (**B**) Corresponding FEs of the O_2//SE//H_2O cell. (**C**) *I-V* curve and FEs for an air//SE//H_2O cell generating pure H_2O_2 solutions. Pure H_2O_2 solutions were generated at a high production rate of 2.3 mmol cm^{-2} $hour^{-1}$ (2490 mol kg_{cat}^{-1} $hour^{-1}$) using only air and water as cathode and anode feedstock, respectively. (**D**) *I-V* curve of the scaled-up unit cell module (80 cm^2 electrode, no *iR* compensation), and (**E**) the corresponding H_2O_2 FEs. (**F**) Dependence of H_2O_2 concentration (up to ~20 wt %) on the DI water flow rate at a constant overall current of 8 A. The data points in (A) to (E) each represent the mean of two independent measurements.

2D), demonstrating the efficacy of the generated H_2O_2 solution in water treatment. A maximal processing rate of 0.88 liter $hour^{-1}$ (0.22 liter $cm^{-2}_{electrode}$ $hour^{-1}$ or 2200 liters $m^{2}_{electrode}$ $hour^{-1}$) was achieved in lowering the TOC level to meet the drinking water standards, making our design economically and environmentally appealing for practical rainwater treatment when scaled up.

We also demonstrated that the oxidation reaction on the anode side could be flexibly modified to be coupled with the cathodic $2e^-$-ORR for applications where H_2 is not available (fig. S14). Water oxidation to O_2 with concurrent proton release might be easier to access than hydrogen oxidation. A 0.5 M aqueous sulfuric acid solution on the anode side was used to lower the ionic resistance; H_2SO_4 was not consumed during the reaction and was continuously circulated (see materials and methods). The CEM membrane blocked crossover of the H_2SO_4 into the porous solid electrolyte layer, ensuring the formation of pure H_2O_2 solutions. This was confirmed by pH and ICP-OES measurements: The pH of the generated H_2O_2 solution was ~6 to 7 (pure H_2O_2 solutions show weak acidity), and the sulfur impurity level was <10 ppm. High H_2O_2 productivity of 3.3 mmol cm^{-2} $hour^{-1}$ (3565 mol kg_{cat}^{-1} $hour^{-1}$) could be achieved at a cell voltage of 2.13 V (Fig. 3A), representing an electricity-to-chemical energy conversion efficiency of 22.6%. H_2O_2 selectivity was very close to that observed with the O_2//SE//H_2 design at comparable current density (Fig. 2B), ruling out any impact on the cathodic $2e^-$-ORR reaction by the anodic water oxidation. The ultrahigh purity of the synthesized H_2O_2 solution was confirmed using ICP-OES. A 100-hour test continuously generated pure H_2O_2 solutions, confirming the robust stability of the O_2//SE//H_2O cell (fig. S15). To further simplify our process, we directly pumped air rather than purified O_2 to the cathode side (Fig. 3C). Although higher cell voltages were required to drive the reaction owing to substantially decreased O_2 concentration and activity, the air//SE//H_2O cell continued to provide H_2O_2 selectivity of >90%. A maximal H_2O_2 partial current of ~123 mA cm^{-2} was reached at 2.71 V, corresponding to an impressive H_2O_2 productivity of 2.3 mmol cm^{-2} $hour^{-1}$ (2490 mol kg_{cat}^{-1} $hour^{-1}$). To validate the scalability of our porous solid electrolyte design, we extended the electrode area from 4 cm^2 used for performance evaluation to ~80 cm^2 in one unit modular cell (Fig. 3, D to F); these could be further stacked in the future for greater capacity. A maximal cell current of >20 A was achieved, with a high H_2O_2 selectivity of ~80% and a production rate of ~0.3 mol $hour^{-1}$. Under a fixed cell current of 8 A, our scaled-up device produced highly concentrated pure H_2O_2 solutions of up to 20 wt % under a DI flow rate of 5.4 ml $hour^{-1}$ (Fig. 3F and fig. S12B).

Given the wide variety of liquid products amenable to electrochemical synthesis, our solid electrolyte design could in principle be extended beyond H_2O_2 generation to other important electrochemical applications.

REFERENCES AND NOTES

1. S. Yang *et al.*, *ACS Catal.* **8**, 4064–4081 (2018).
2. Y. Yi, L. Wang, G. Li, H. Guo, *Catal. Sci. Technol.* **6**, 1593–1610 (2016).
3. R. J. Lewis, G. J. Hutchings, *ChemCatChem* **11**, 298–308 (2019).
4. J. K. Edwards, G. J. Hutchings, *Angew. Chem. Int. Ed.* **47**, 9192–9198 (2008).
5. J. H. Lunsford, *J. Catal.* **216**, 455–460 (2003).
6. D. P. Dissanayake, J. H. Lunsford, *J. Catal.* **206**, 173–176 (2002).
7. J. K. Edwards *et al.*, *Science* **323**, 1037–1041 (2009).
8. J. K. Edwards *et al.*, *Angew. Chem. Int. Ed.* **48**, 8512–8515 (2009).
9. S. J. Freakley *et al.*, *Science* **351**, 965–968 (2016).
10. Q. Liu, J. C. Bauer, R. E. Schaak, J. H. Lunsford, *Appl. Catal. A Gen.* **339**, 130–136 (2008).
11. S. Abate *et al.*, *Catal. Today* **157**, 280–285 (2010).
12. Q. Liu, J. C. Bauer, R. E. Schaak, J. H. Lunsford, *Angew. Chem. Int. Ed.* **47**, 6221–6224 (2008).
13. C. E. Baukal Jr., *Oxygen-Enhanced Combustion* (CRC, 2013).
14. S. Siahrostami *et al.*, *Nat. Mater.* **12**, 1137–1143 (2013).
15. H. W. Kim *et al.*, *Nat. Catal.* **1**, 282–290 (2018).
16. Z. Lu *et al.*, *Nat. Catal.* **1**, 156–162 (2018).
17. S. Chen *et al.*, *J. Am. Chem. Soc.* **140**, 7851–7859 (2018).
18. S. Chen *et al.*, *ACS Sustain. Chem. Eng.* **6**, 311–317 (2017).
19. I. Yamanaka, T. Murayama, *Angew. Chem. Int. Ed.* **47**, 1900–1902 (2008).
20. W. Li, A. Bonakdarpour, E. Gyenge, D. P. Wilkinson, *ChemSusChem* **6**, 2137–2143 (2013).
21. W. T. Li, A. Bonakdarpour, E. Gyenge, D. P. Wilkinson, *J. Appl. Electrochem.* **48**, 985–993 (2018).
22. X. Tian, P. Zhao, W. Sheng, *Adv. Mater.* **31**, 1808066 (2019).
23. W. Sheng, H. A. Gasteiger, Y. Shao-Horn, *J. Electrochem. Soc.* **157**, B1529–B1536 (2010).
24. M. S. Wilson, S. Gottesfeld, *J. Electrochem. Soc.* **139**, L28–L30 (1992).
25. J. S. Jirkovský *et al.*, *J. Am. Chem. Soc.* **133**, 19432–19441 (2011).
26. L. Han *et al.*, *ACS Catal.* **9**, 1283–1288 (2019).
27. D. Iglesias *et al.*, *Chem* **4**, 106–123 (2018).
28. T.-P. Fellinger, F. Hasché, P. Strasser, M. Antonietti, *J. Am. Chem. Soc.* **134**, 4072–4075 (2012).
29. Y. Liu, X. Quan, X. Fan, H. Wang, S. Chen, *Angew. Chem. Int. Ed.* **54**, 6837–6841 (2015).
30. S. C. Perry *et al.*, *Nat. Rev. Chem.* **3**, 442–458 (2019).
31. S. Günday, A. Bozkurt, W. H. Meyer, G. Wegner, *J. Polym. Sci. B* **44**, 3315–3322 (2006).
32. W. A. England, M. Cross, A. Hamnett, P. Wiseman, J. B. Goodenough, *Solid State Ion.* **1**, 231–249 (1980).
33. L. Fan, S. Wei, S. Li, Q. Li, Y. Lu, *Adv. Energy Mater.* **8**, 1702657 (2018).
34. Q. Zhao, X. Liu, S. Stalin, K. Khan, L. A. Archer, *Nat. Energy* **4**, 365–373 (2019).
35. S. H. Lee, J. C. Rasaiah, *J. Chem. Phys.* **135**, 124505 (2011).
36. F. M. Coutinho, S. M. Rezende, B. G. Soares, *J. Appl. Polym. Sci.* **102**, 3616–3627 (2006).
37. R. C. Weast, M. J. Astle, W. H. Beyer, *CRC Handbook of Chemistry and Physics* (CRC, 1988), vol. 69.
38. K. J. Jeong *et al.*, *J. Power Sources* **168**, 119–125 (2007).
39. Z. M. Galbács, L. J. Csányi, *J. Chem. Soc., Dalton Trans.* **11**, 2353–2357 (1983).
40. M. Ravikumar, A. Shukla, *J. Electrochem. Soc.* **143**, 2601–2606 (1996).
41. B. D. Black, G. W. Harrington, P. C. Singer, *J. Am. Water Works Assoc.* **88**, 40–52 (1996).
42. A. Wenzel, A. Gahr, R. Niessner, *Water Res.* **33**, 937–946 (1999).
43. Texas Commission on Environmental Quality, *Total Organic Carbon (TOC) Guidance Manual*; https://tceq.texas.gov/assets/public/comm_exec/pubs/rg/rg-379.pdf.
44. D. W. Flaherty, *ACS Catal.* **8**, 1520–1527 (2018).
45. P. Biasi *et al.*, *Chem. Eng. J.* **176–177**, 172–177 (2011).
46. J. Zhang *et al.*, *Small* **14**, 1703990 (2018).
47. F. Li, Q. Shao, M. Hu, Y. Chen, X. Huang, *ACS Catal.* **8**, 3418–3423 (2018).
48. I. Yamanaka, T. Hashimoto, R. Ichihashi, K. Otsuka, *Electrochim. Acta* **53**, 4824–4832 (2008).
49. I. Yamanaka, T. Onizawa, S. Takenaka, K. Otsuka, *Angew. Chem. Int. Ed.* **42**, 3653–3655 (2003).
50. I. Yamanaka, T. Onizawa, H. Suzuki, N. Hanaizumi, K. Otsuka, *Chem. Lett.* **35**, 1330–1331 (2006).
51. H. J. Luo, C. L. Li, C. Q. Wu, X. Q. Dong, *RSC Advances* **5**, 65227–65235 (2015).
52. A. Da Pozzo, L. Di Palma, C. Merli, E. Petrucci, *J. Appl. Electrochem.* **35**, 413–419 (2005).
53. Z. Chen *et al.*, *React. Chem. Eng.* **2**, 239–245 (2017).

ACKNOWLEDGMENTS

Funding: This work was supported by Rice University. H.W. is a CIFAR Azrieli Global Scholar in the Bio-inspired Solar Energy Program. C.X. acknowledges support from a J. Evans Attwell-Welch Postdoctoral Fellowship provided by the Smalley-Curl Institute. **Author contributions:** C.X. and H.W. conceptualized the project. H.W. supervised the project. C.X. synthesized carbon black catalysts with the help of Y.X. C.X. and Y.X. conducted the catalytic tests and the related data processing. C.X. performed materials characterization and analysis with the help of P.Z. L.F. designed the schemes. C.X. and H.W. wrote the manuscript. **Competing interests:** A U.S. provisional patent application (no. 62/874,176) based on the technology described in this work was filed on 15 July 2019 by C.X. and H.W. at Rice University. The other authors declare no competing interests. **Data and materials availability:** All experimental data are available in the main text or the supplementary materials.

SUPPLEMENTARY MATERIALS

science.sciencemag.org/content/366/6462/226/suppl/DC1
Materials and Methods
Figs. S1 to S15
Table S1
Supplementary Text
References (*54*–*67*)

27 May 2019; accepted 16 September 2019
10.1126/science.aay1844

Science

Direct electrosynthesis of pure aqueous H_2O_2 solutions up to 20% by weight using a solid electrolyte

Chuan Xia, Yang Xia, Peng Zhu, Lei Fan and Haotian Wang

Science **366** (6462), 226-231.
DOI: 10.1126/science.aay1844

A direct route to pure peroxide

Despite the widespread use of hydrogen peroxide as an oxidant and disinfectant, its commercial synthesis still requires inefficient concentration and purification steps. Xia *et al.* now report an electrochemical approach to synthesizing pure peroxide solutions straight from hydrogen and oxygen. Using a solid-state electrolyte, they avoid contamination of the product solution by extraneous ions. Varying the flow rate of water through the electrochemical cell tunes the final concentration over a range from 0.3% to 20% by weight.

Science, this issue p. 226